Acta Crystallographica Section B
Structural Science
ISSN 0108-7681

Molecular origins of commercial laser dye functionality in azacoumarins and 2-quinolones: LD 425, LD 489 and LD 473

Xiaogang Liu,[a] Jacqueline M. Cole,[a,b,c]* Paul G. Waddell[a,b] and Tze-Chia Lin[a]

[a]Cavendish Laboratory, Department of Physics, University of Cambridge, J. J. Thomson Avenue, Cambridge CB3 0HE, England, [b]Department of Chemistry, University of New Brunswick, PO Box 4400, Fredericton, NB E3B 5A3, Canada, and [c]Department of Physics, University of New Brunswick, PO Box 4400, Fredericton, NB E3B 5A3, Canada

Correspondence e-mail: jmc61@cam.ac.uk

Received 9 June 2011
Accepted 13 September 2011

The molecular structures of three compounds, LD 425 ($C_{13}H_{14}N_2O_3$) (1), LD 489 ($C_{15}H_{15}F_3N_2O_2$) (2) and LD 473 ($C_{17}H_{19}F_3N_2O$) (3), are determined by single-crystal X-ray diffraction (XRD) at 180 K. Azacoumarins (1) and (2) possess *para*-quinoidal bond-length patterns in their benzene rings due to intramolecular charge transfer (ICT) from these rings to the adjoining rings. In contrast, substitution of O with N within the coumarin heterocycle, to form a 2-quinolone, results in the suppression of this ICT effect. Instead, charge transfer within the heterocycle is shown to become more pronounced. Resonance theory is employed to discuss these bond pattern differences and characteristic spectral blue shifts in relation to their coumarin analogues. The application of this theory offers an intuitive understanding of the structure–property relationships in azacoumarins and 2-quinolones which is further supported by quantum chemical calculations. Such an understanding is important for recognizing ICT mechanisms in these compounds which can then be used to facilitate the molecular design of new laser dyes with the desired spectral shifts.

1. Introduction

Azacoumarins and 2-quinolones are used in a wide range of applications, such as laser dyes (Fletcher *et al.*, 1987; Hammond *et al.*, 1975, 1978*a*,*b*) and as biodynamic agents and inhibitors (Allen, Biswas *et al.*, 2009; Allen, Burli *et al.*, 2009; Kulkarni *et al.*, 2006). Although their synthesis has been discussed extensively (Allen, Biswas *et al.*, 2009; Allen, Burli *et al.*, 2009; Dalla Via *et al.*, 2002; Hammond *et al.*, 1978*a*,*b*; Lapiere, 1975), relatively few crystal structures have been reported compared with their structurally close analogues, coumarins. For example, a search in the Cambridge Structural Database (CSD; Allen, 2002) returned no records for azacoumarins and 155 records for 2-quinolones. In contrast, there were 746 records for organic coumarin derivatives alone. This fundamental dearth of crystallographic information is perhaps more surprising when considering that some of these azacoumarins and 2-quinolones are in active industrial application, such as dye lasers. In this paper, the crystal structures of three compounds are reported: namely LD 425 ($C_{13}H_{14}N_2O_3$; 4-methyl-7-morpholino-2*H*-pyrano[2,3-b]pyridin-2-one) (1), LD 489 ($C_{15}H_{15}F_3N_2O_2$; 6,7,8,9-tetrahydro-(6*S*,8*R*)-6,8,9-trimethyl-4-(trifluoromethyl)-2*H*-pyrano[2,3-b]-[1,8]naphthyridin-2-one) (2) and LD 473 ($C_{17}H_{19}F_3N_2O$; (*R*)-1,2,3,3,8-pentamethyl-5-(trifluoromethyl)-2,3-dihydro-1*H*-pyrrolo[3,2-g]quinolin-7(8*H*)-one) (3). Compounds (1) and (2) belong to the family of azacoumarins, while (3) is a 2-quinolone. Azacoumarin and 2-quinolone laser dyes have shorter

© 2011 International Union of Crystallography
Printed in Singapore – all rights reserved

Table 1
Crystal data collection and refinement parameters for the title compounds.

For all structures: monoclinic, $P2_1/c$. Experiments were carried out at 180 K with Mo $K\alpha$ radiation. Refinement was undertaken with no restraint. The coordinates of all H-atoms were refined freely.

	(1) LD 425	(2) LD 489	(3) LD 473
Crystal data			
Chemical formula	$C_{13}H_{14}N_2O_3$	$C_{15}H_{15}F_3N_2O_2$	$C_{17}H_{19}F_3N_2O$
M_r	246.26	312.29	324.34
a, b, c (Å)	7.061 (5), 24.489 (15), 13.930 (9)	8.9941 (5), 11.2954 (6), 14.3536 (9)	12.1853 (5), 12.2242 (4), 10.6361 (3)
β (°)	103.481 (8)	102.537 (3)	93.4529 (11)
V (Å^3)	2342 (3)	1423.44 (14)	1581.43 (9)
Z	8	4	4
μ (mm^{-1})	0.10	0.12	0.11
Crystal size (mm)	0.56 × 0.28 × 0.11	0.42 × 0.22 × 0.14	0.32 × 0.16 × 0.12
Data collection			
Diffractometer	Rigaku Saturn 724+ CCD diffractometer with SHINE Optics	Nonius KappaCCD	Nonius KappaCCD
Absorption correction	Multi-scan (Blessing, 1997)	Multi-scan (Blessing, 1997)	Multi-scan (Blessing, 1997)
T_{min}, T_{max}	0.973, 1.028	0.958, 0.998	0.943, 0.989
No. of measured, independent and observed [$I > 2\sigma(I)$] reflections	14 043, 5763, 4634	7357, 3199, 2235	14 885, 3601, 2179
R_{int}	0.077	0.032	0.062
$(\sin\theta/\lambda)_{max}$ (Å^{-1})	0.667	0.647	0.649
Refinement			
$R[F^2 > 2\sigma(F^2)]$, $wR(F^2)$, S	0.062, 0.158, 1.13	0.048, 0.127, 1.04	0.048, 0.123, 1.00
No. of reflections	5763	3199	3601
No. of parameters	437	259	284
$\Delta\rho_{max}$, $\Delta\rho_{min}$ (e Å^{-3})	0.31, −0.49	0.31, −0.25	0.22, −0.28

Computer programs used: Rigaku *CrystalClear-SM Expert* 2.0 r4 (Rigaku/MSC, 2009), *COLLECT* (Nonius, 1998), *HKL DENZO and SCALEPACK* (Otwinowski & Minor, 1997), *SHELXS*97, *SHELXL*97 (Sheldrick, 2008), *ORTEP-3 for Windows* (Farrugia, 1997), *publCIF* (Westrip, 2010).

fluorescent/lasing wavelengths than coumarins (Schimitschek & Trias, 1976; Atkins & Bliss, 1978; Hammond *et al.*, 1975). It will be demonstrated that resonance theory provides a good interpretation to link this blue shift to their molecular structures.

2. Experimental

2.1. Sample preparation

The title compounds were supplied by Exciton Chemical Co. Crystals of (1) suitable for single-crystal X-ray crystallography were grown *via* slow diffusion of diethyl ether into a solution of the compound in dichloromethane at room temperature. Crystals of (2) and (3) were grown *via* slow solvent evaporation in methanol at room temperature.

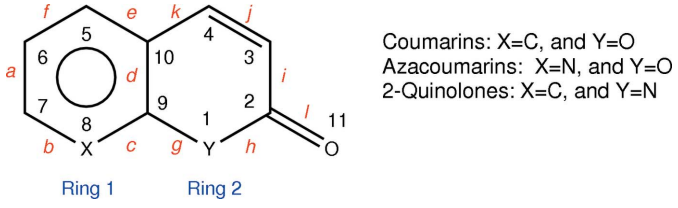

Figure 1
Designation of molecular parameter descriptors.

2.2. X-ray crystallography

For (1) data were collected at 180 K on a Rigaku Saturn 724+ CCD diffractometer equipped with a molybdenum X-ray source [λ(Mo $K\alpha$) = 0.71073 Å] and accompanying SHINE Optics. An open-flow nitrogen Oxford Cryosystems Cryostream Plus was used to cool the sample. Rigaku *CrystalClear-SM Expert* 2.0 (Rigaku/MSC, 2009) software was used for all data collection, cell refinement and data reduction procedures.

For (2) and (3) data were collected at 180 K on a Nonius KappaCCD area-detector diffractometer equipped with a Mo $K\alpha$ X-ray source and an open-flow nitrogen Oxford Cryosystems Cryostream. Data collection employed the software *COLLECT* (Nonius, 1998); cell refinement and data reduction were conducted using software *HKL DENZO* and *SCALEPACK* (Otwinowski & Minor, 1997).

A summary of crystal, data collection and refinement details is given in Table 1.[1]

2.3. Cambridge Structural Database enquiries

The structural data of all compounds containing coumarin, azacoumarin and 2-quinolone fragments were sought *via* the CSD, Version 2010 (Allen, 2002), using *ConQuest* 1.13 (Bruno *et al.*, 2002). This enabled the study of the overall bond pattern

[1] Supplementary data for this paper are available from the IUCr electronic archives (Reference: BK5105). Services for accessing these data are described at the back of the journal.

Table 2
Selected bond distances (Å) for the title compounds.

	$C_{13}H_{14}N_2O_3$ (1)			
Bond	Molecule 1	Molecule 2	$C_{15}H_{15}F_3N_2O_2$ (2)	$C_{17}H_{19}F_3N_2O$ (3)
a	1.414 (3)	1.419 (2)	1.433 (2)	1.412 (2)
b	1.350 (2)	1.349 (2)	1.343 (2)	1.377 (2)
c	1.324 (2)	1.322 (2)	1.314 (2)	1.411 (2)
d	1.394 (2)	1.398 (2)	1.391 (2)	1.420 (2)
e	1.403 (2)	1.407 (2)	1.416 (2)	1.419 (2)
f	1.377 (2)	1.372 (2)	1.366 (2)	1.359 (2)
g	1.377 (2)	1.374 (2)	1.377 (2)	1.395 (2)
h	1.383 (2)	1.385 (2)	1.3820 (19)	1.387 (2)
i	1.444 (2)	1.440 (2)	1.435 (2)	1.437 (2)
j	1.349 (2)	1.349 (2)	1.354 (2)	1.345 (2)
k	1.445 (2)	1.445 (2)	1.434 (2)	1.432 (2)
l	1.217 (2)	1.214 (2)	1.215 (2)	1.236 (2)

shifts among these three classes of chemical families. The following restrictions were applied during the search:

(i) three-dimensional atomic coordinates were available;

(ii) the crystal was not ionic;

(iii) only organic compounds were considered.

There were 746, 155 and 0 records returned for coumarins, 2-quinolones and azacoumarins.

All structural searches employed bond labelling as shown in Fig. 1. Common to all three families is an aromatic ring (Ring 1), fused with a second ring (Ring 2) which contains a double bond, *j*, such that it extends the π-conjugated system across the molecule in coumarins, azacoumarins and 2-quinolones.

The coumarin and 2-quinolone data records were further screened based on the following two criteria:

(i) Only homomolecular crystals were considered. Hydrates, solvates and co-crystal systems were omitted to avoid any possible bias in the bond lengths of these compounds, as a result of interactions between distinct molecular species. Such interactions could significantly deform the bond patterns of coumarins and 2-quinolones. For example, in coumarin 4 monohydrate the ketone group is much more elongated compared with anhydrous coumarin 4 (Butcher *et al.*, 2007; Jasinski & Woudenberg, 1994; Shimizu *et al.*, 1975; Yang *et al.*, 2007).

(ii) If $Z' > 1$ the average bond lengths of these molecules were used in our analysis.

As a result of this screening, 653 and 134 sets of bond length data became available for coumarins and 2-quinolones.

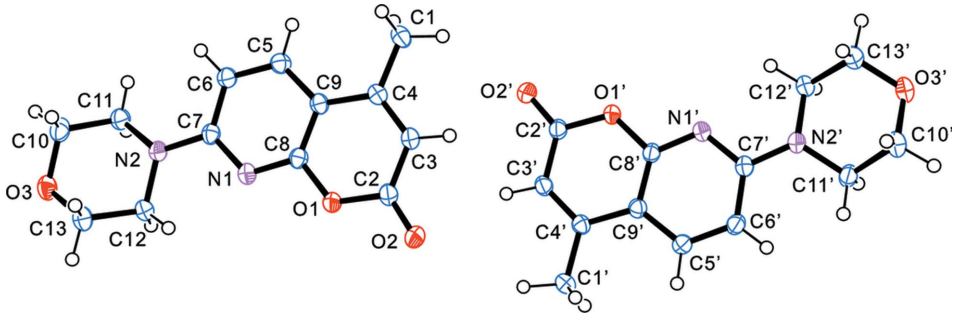

Figure 2
The asymmetric unit of (1) with anisotropic displacement ellipsoids drawn at the 50% probability level.

2.4. Quantum chemical calculations

Quantum chemical calculations were performed on selected compounds (§3.4) from the three chemical families of coumarins, azacoumarins and 2-quinolones using *GAUSSIAN*09 (Frisch *et al.*, 2009). This enabled a comparison of band gaps and the nature of electronic charge transfer upon photo-excitation in these compounds to be studied.

The geometries of these molecules were optimized with density functional theory (DFT) using Becke's three-parameter hybrid functional B3LYP and a 6-31G(d) basis set (Lee *et al.*, 1988; Becke, 1993; Stephens *et al.*, 1994). The highest occupied molecular orbitals (HOMO) and lowest unoccupied molecular orbitals (LUMO) of these compounds were calculated with time-dependent density functional theory (TD-DFT) using the hybrid Perdew, Bruke and Ernzerhof functional (PBE1PBE) and a 6-31++G(d,p) basis set (Adamo & Barone, 1999).

3. Results and discussions

Anisotropic displacement ellipsoid plots at 50% probability for (1)–(3) are given in Figs. 2–4, respectively. Selected bond lengths for each compound are given in Table 2.

Resonance theory, which successfully explains *para*-quinoidal structures in coumarins (Cole *et al.*, 2011), can also be used to elucidate structural patterns in azacoumarins and 2-quinolones since these three families of compounds are closely related. With this theory, all possible resonance structures (canonical forms) in a π-conjugated molecular system can be identified. By comparing these canonical forms with a molecular structure obtained from an XRD experiment, we can determine the dominant resonance structures and attain a first-order approximation on major ICT within the molecule. Such analysis based on structural data is simple and intuitive, and yet offers an effective method for understanding certain electronic properties of molecules, such as their UV–vis absorption and fluorescence spectra.

3.1. Para-quinoidal structures in azacoumarins (1) and (2)

There are two major structural features of interest in (1) and (2). Firstly, their bonds *c* and *f* are much shorter compared with their neighbouring bonds, which leads Ring 1 to exhibit a *para*-quinoidal structure. While it may not be fair to compare the length of bond *c* with its neighbour *d* due to the different bond types involved (C⋯N *versus* C⋯C), it is clear that bond *c* is markedly short among carbon–nitrogen bonds in Ring 1, as shown by a comparison of bonds *c* and *b* (Table 2). In fact, bond *c* is much shorter than the average C⋯N length of 1.337 Å in pyridine, whereas bond *b* is longer (Allen *et al.*, 1987). Secondly, a strong electron-donating amino group is

Table 3
Geometric data related to the C7—N2 bonds at the 7-position substituents for the title compounds.

$C_{13}H_{14}N_2O_3$ (1)		$C_{15}H_{15}F_3N_2O_2$ (2)		$C_{17}H_{19}F_3N_2O$ (3)	
Bond lengths (Å)					
C7—N2	1.376 (2)	C7—N2	1.356 (2)	C7—N2	1.380 (2)
C7′—N2′	1.367 (2)				
Torsion angles (°)					
C6—C7—N2—C11	11.6 (3)	C6—C7—N2—C11	−1.4 (3)	C6—C7—N2—C11	−18.60 (19)
N1—C7—N2—C12	−15.8 (3)	N1—C7—N2—C12	11.7 (3)	C8—C7—N2—C12	20.5 (3)
χ_N	**27.4 (4)**	χ_N	**13.1 (4)**	χ_N	**39.1 (4)**
C6′—C7′—N2′—C11′	20.3 (3)				
N1′—C7′—N2′—C12′	−6.8 (3)				
χ'_N	**27.1 (4)**				

attached to the 7-position in both (1) and (2). This enhances the ICT from Ring 1 to Ring 2. The net effect is the stabilization of *para*-quinoidal resonance structure (5*b*) (Fig. 5) in azacoumarins, since this substituent extends the π-conjugated bonding through the *para*-quinoidal structure of Ring 1 to the *para*-position (bond *k*). A similar trend is observed in coumarin laser dyes (Cole *et al.*, 2011). Indeed, such a structural modification is a widely adopted strategy for improving optical properties in laser dyes (Duarte & Hillman, 1990).

The presence of the *para*-quinoidal resonance structure (5*b*) is also reflected by the partial double-bond nature of the C7—N2 bond in the 7-position substituent (Table 3). Firstly, the N2 atom lies close to the Ring 1 plane, with displacements of 0.051–0.069 Å for (1) and 0.082 Å for (2). Furthermore, this C7—N2 bond length (Table 3) lies between those of pure single and double carbon–nitrogen bonds, which are typically 1.44 and 1.27 Å (Gilli *et al.*, 1986). Lastly, the torsion angles involving the C7—N2 bond (Table 3) also suggest the partial sp^2 hybridization of the N atom and the alignment of the nitrogen lone pair with the π-system of Ring 1: the total torsion angle, χ_N, denotes the absolute value of the difference between the two torsion angles along the C7—N2 bond. This angle represents the overall out-of-plane torsion angle of the two substituent branches attached to the N2 atom with respect to the Ring 1 plane, as N2 lies almost in this plane; it ranges from 0° for perfect planar sp^2 to 60° for idealized tetrahedral sp^3 nitrogen hybridization (Gilli *et al.*, 1986). In both (1) and (2) this angle is less than 30° and more akin to sp^2 hybridization (Table 3). In summary, the close alignment of the N atom (N2) to the Ring 1 plane, the C7—N2 bond lengths lying intermediate to typical single and double bond lengths, and the relatively small χ_N values all suggest the partial double-bond nature of the C7—N2 bonds and support the resonance structures proposed in Fig. 5.

Resonance theory works equally well to explain the bond lengths in Ring 2. Owing to the contribution of resonance structure (5*a*) (Fig. 5), bonds *i* and *k* are longer than bond *j*. However, our crystallographic data (Table 2) show that bonds *i* and *k* in azacoumarins are shorter than the average single bond length between aromatic and sp^2 hybridized C atoms of 1.470 Å (Allen *et al.*, 1987). This bond-length shortening can be explained by the competing influence from resonance structure (5*b*). Nevertheless, the contribution of (5*b*) is relatively small and bonds *i* and *k* are still more akin to a single

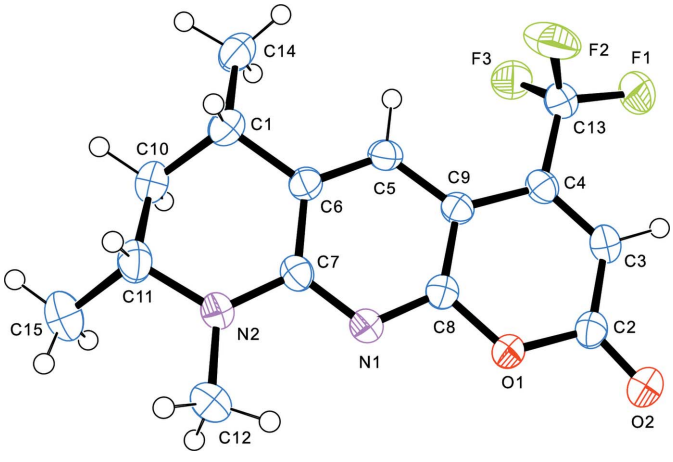

Figure 3
The molecular structure of (2) with anisotropic displacement ellipsoids drawn at the 50% probability level.

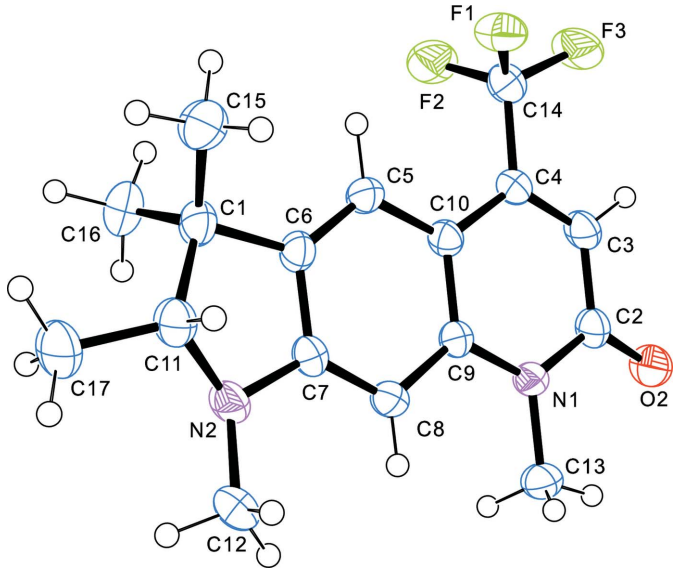

Figure 4
The molecular structure of (3) with anisotropic displacement ellipsoids drawn at the 50% probability level.

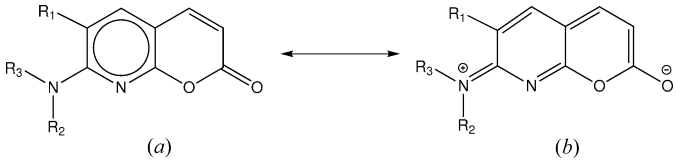

Figure 5
Dominant resonance structures in azacoumarins.

bond, while *j* is more representative of a double bond. For the same reason, bond *l* (Table 2) is slightly longer than the average length of C═O bonds in esters (1.199 Å) with similar bond-type geometries (Allen *et al.*, 1987).

3.2. Resonance structures of 2-quinolone (3)

The *para*-quinoidal structure is not observed in the 2-quinolone (3). In (3) bond *c* is longer than bond *b* by 0.034 (3) Å, despite the fact that an electron-donating amino group is also attached to its 7-position. In fact, although N2 from this amino group also lies in the Ring 1 plane (with a tiny offset of 0.007 Å), its electron-donating strength is not as strong as in its azacoumarin analogues (1) and (2). This is reflected by the reduced double-bond character of C7—N2 in (3): this bond of 1.380 (2) Å in (3) is longer than in (1) and (2) (Table 3); moreover, the total torsion angle, χ_N, is as high as 39.1 (4)° in (3). This large angle shows that the N2 hybridization is more prone to the tetrahedral sp^3 nitrogen hybridization ($\chi_N = 60°$) than the planar sp^2 nitrogen hybridization ($\chi_N = 0°$). In other words, the lone pair from N2 in (3) is not as well aligned with the π-system of Ring 1 in contrast to in (1) and (2).

Instead, another pair of resonance structures, which features electron transfer between N1 and O2, is significant in (3) (Fig. 6). The significance of these resonance states can be rationalized by considering that in 2-quinolones, the O atom located at the 1-position in coumarins has been replaced by N1. Consequently, the strong electron-donating ability of N1 has a greater influence on the competing resonances. This effect is reflected in the bond-length pattern of (3): in Ring 2 bond *h* is relatively short, while bond *l* is slightly elongated compared with average lengths in similar bond-type geometries (Allen *et al.*, 1987) due to the influence of the resonance state (6*b*) (Fig. 6). Correspondingly, bond *h* is shorter than *g*; bond *l* is more than 0.019 (3) Å longer than in (1) and (2) (Table 2).

Lastly, it should be pointed out that the crystal structural data of (3) at room temperature have already been published with the CSD reference code VIGXAK (Chinnakali *et al.*, 1991). However, our data was collected at 180 K in order to reduce atomic thermal vibrations and to ensure consistency in our data presented herein by having a common temperature for data collection. Our resulting data contain smaller standard deviations in bond lengths and angles compared with the VIGXAK study. These deviations are averaged at 0.002 Å and 0.1° for bonds not containing H atoms *versus* 0.004 Å and 0.2° in VIGXAK. Other than that, these two data sets agree with each other reasonably well, with the largest bond-length difference being 0.012 (4) Å for C14—F3, and the largest bond-angle variance being 0.8 (2)° for C10—C4—C14.

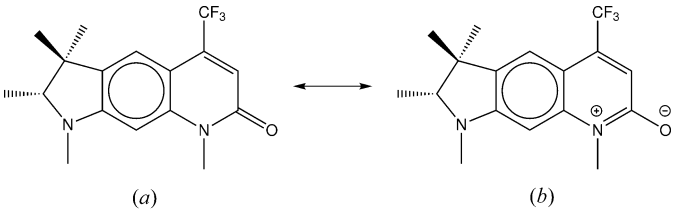

Figure 6
Significant resonance structures in 2-quinolone (3).

3.3. Comparison of bond-length patterns in coumarins and 2-quinolones

The resonance states which feature marked electron transfer between N1 and O2 are not exclusive to (3), but are observed in a wide range of 2-quinolones. To study the structural changes in 2-quinolones, the bond lengths of 653 coumarins and 134 2-quinolones were compared. During this comparison, only low-temperature data should ideally be considered, because they involve reduced atomic thermal vibrations and are more accurate. In addition, such data should be collected at preferably similar temperatures in order to minimize bias from temperature effects. Unfortunately, relatively few structural data for coumarins and 2-quinolones have been obtained at low temperature, and their experimental temperatures vary considerably – from 90 to 230 K (Fig. 7). In contrast, most of these structural data (including 514 coumarins and 106 2-quinolones) are collected at (or near) room temperature from 273 to 300 K. These bond lengths contain relatively large errors. Nevertheless, we are concerned with the differences of overall bond length *patterns* in coumarins and 2-quinolones, and the general pattern variance between the two classes of chemical families is still observable given the large sample size of the room-temperature data. For these reasons, a bond-length pattern comparison based on the room-temperature data is presented here. A more comprehensive map of resonance states in coumarins and 2-quinolones has also been plotted to explain the structural variance (Fig. 8).

The largest bond-length difference in Ring 1 between these two families of compounds concerns bond *c* [Fig. 9, (I)]. Bond *c* is relatively short in coumarins due to the contribution from the *para*-quinoidal structure (III) observed in many laser dye

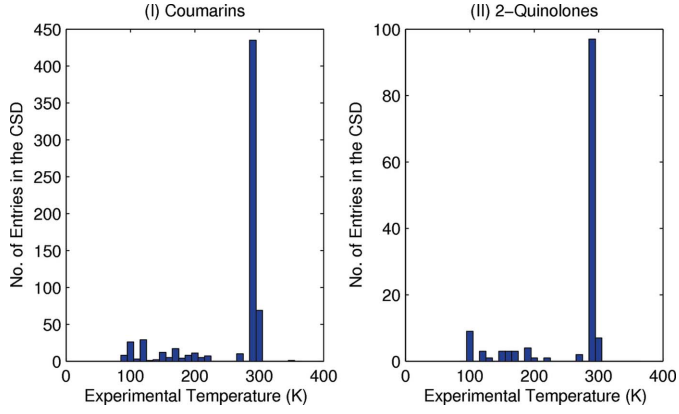

Figure 7
The experimental temperature profile of XRD data for (I) coumarins and (II) 2-quinolones.

coumarins (Fig. 8; Cole *et al.*, 2011). On the other hand, bond *c* in 2-quinolones is longer than bond *b* by an average of 0.023 Å. This difference indicates the absence of the *para*-quinoidal form in 2-quinolones due to the diminution of ICT from Ring 1 to Ring 2. In fact, only one of the 134 2-quinolones has a strong electron-donating substituent at the 7-position; in that case the ICT effect is still weak, as observed in (3). The impact of resonance state (III) on the bond patterns of 2-quinolones is therefore insignificant. Another important feature in Ring 1 is related to resonance state (I) (Fig. 8). The influence of this state is largely the cause of bonds *b* and *f* being relatively short in both coumarins and 2-quinolones with respect to other bonds in Ring 1.

The most noteworthy difference in Ring 2 lies at bond *l* [C2═O2; Fig. 9, (II)]. The average length of this bond is elongated by 0.029 Å in 2-quinolones compared with that in coumarins. This reflects a greater contribution from the resonance states (I), (V) and (VI) in the structure of 2-quinolones (Fig. 8). The second notable feature is related to bond *h*. As *h* is of different bond types in coumarins and 2-quinolones, it is less meaningful to directly compare its length between the two chemical families. Therefore, the differences between bonds *g* and *h* in coumarins and 2-quinolones are computed instead [Fig. 9, (III)]. Such differences are centred around 0 for coumarins, while these values for 2-quinolones have a positive shift of 0.010 Å, on average. This shift is caused by the shortening of bond *h* compared with *g*. Both resonance states (V) and (VI) have contributed to this change positively, while state (I) contributes negatively. This competition between resonance states explains why the shortening of bond *h* is not as substantial as the elongation of bond *l*.

However, it should be remembered that the above discussion concerns the average bond patterns in coumarins and 2-quinolones. Bond-length variations in *g* and *h* will depend on other substituents on Ring 2 as additional resonance structures may become possible in such events.

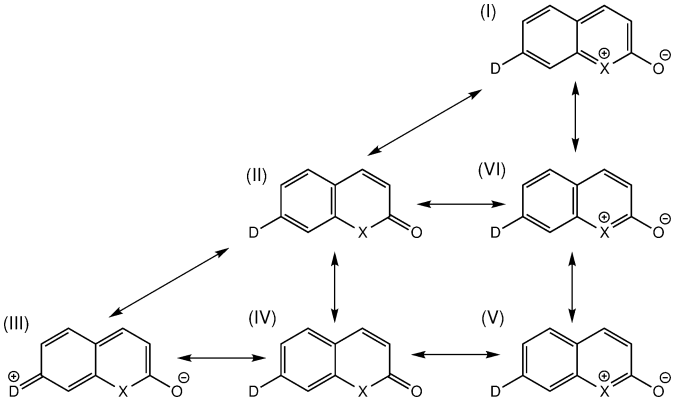

Figure 8
Possible resonance structures in coumarins and 2-quinolones. Atom *X* represents oxygen in coumarins and nitrogen in 2-quinolones. While only the 7-position electron-donating substituent *D* is shown here, other substituents are likely to be attached onto this framework. It is also possible to have no substituent at the 7-position, in which case resonance state (III) is not applicable any more.

It is also worth mentioning that the low-temperature structural data exhibit the same bond patterns. We have divided the low-temperature data into three groups – Group 1 between 90 and 129 K, Group 2 between 130 and 179 K and Group 3 between 180 and 229 K. The reduced temperature variance in each of the groups helps to diminish possible bias from temperature effects. The bond-length patterns between coumarins and 2-quinolones in these groups afforded the same pattern to the room-temperature data, thus corroborating this pattern analysis. The detailed results are presented in *Appendix A*.

3.4. Structure–property relationships – wavelength shifts in UV–vis absorption and emission spectra

The excitation of laser dyes composed of coumarins, azacoumarins and 2-quinolones induces ICT from Ring 1 (donor) to Ring 2 (acceptor). This effect not only alters the bond lengths of these molecules, but it also has a large impact on their electronic band gaps. This is because the ICT can be assisted by elevating the energy of the donor level in Ring 1,

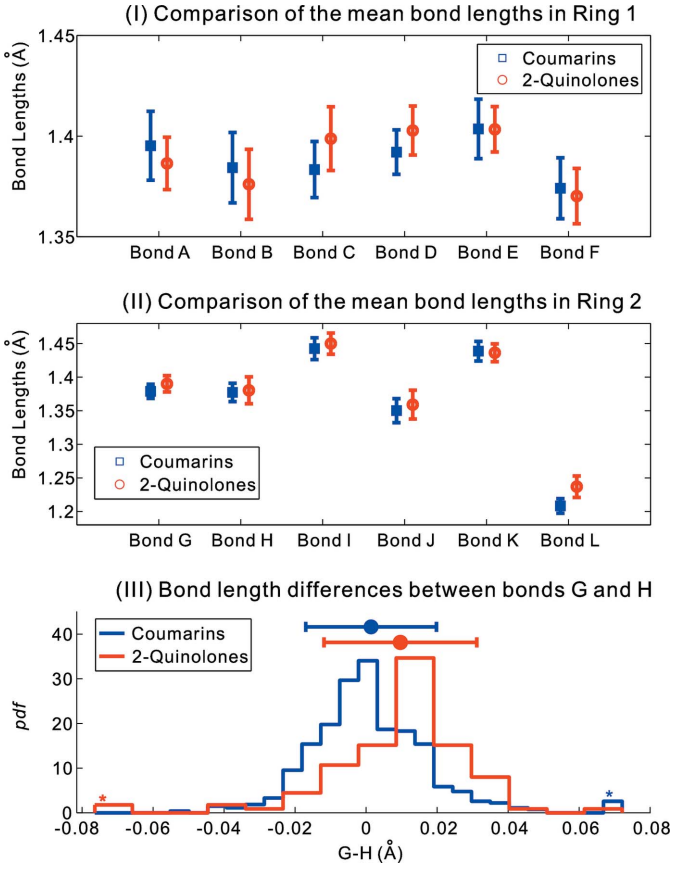

Figure 9
Comparison of average bond lengths in coumarins and 2-quinolones in the room-temperature group. The expected values with their standard deviations (2σ) are plotted in (I) and (II) for Ring 1 and Ring 2, respectively. The differences between bonds *g* and *h* are computed and plotted as a probability density function (p.d.f.) in (III). Such differences are centred at around 0 for coumarins, while bond *h* is shorter than bond *g* in most 2-quinolones.

Table 4
Average bond lengths of coumarins and 2-quinolones with structural data collected between 90 and 129 K.

	Ring 1						
	Bond *a*	Bond *b*	Bond *c*	Bond *d*	Bond *e*	Bond *f*	Sample size
Coumarins	1.4045 (139)	1.3884 (156)	1.3857 (84)	1.3954 (80)	1.4071 (98)	1.3808 (117)	66
2-Quinolones	1.3970 (88)	1.3772 (48)	1.4020 (96)	1.4070 (79)	1.4077 (65)	1.3713 (96)	12

	Ring 2						
	Bond *g*	Bond *h*	Bond *i*	Bond *j*	Bond *k*	Bond *l*	Bonds *G*–*H*
Coumarins	1.3775 (66)	1.3788 (89)	1.4506 (126)	1.3534 (119)	1.4386 (134)	1.2109 (68)	−0.0013
2-Quinolones	1.3903 (117)	1.3684 (196)	1.4515 (171)	1.3665 (130)	1.4367 (94)	1.2503 (175)	0.0220

Table 5
Average bond lengths of coumarins and 2-quinolones with structural data collected between 130 and 179 K.

	Ring 1						
	Bond *a*	Bond *b*	Bond *c*	Bond *d*	Bond *e*	Bond *f*	Sample size
Coumarins	1.3989 (179)	1.3863 (153)	1.3859 (94)	1.3955 (93)	1.4026 (87)	1.3778 (127)	37
2-Quinolones	1.3998 (158)	1.3938 (220)	1.4158 (222)	1.4015 (102)	1.4156 (85)	1.3614 (189)	10

	Ring 2						
	Bond *g*	Bond *h*	Bond *i*	Bond *j*	Bond *k*	Bond *l*	Bonds *G*–*H*
Coumarins	1.3789 (77)	1.3784 (125)	1.4505 (106)	1.3545 (172)	1.4388 (189)	1.2107 (86)	0.0005
2-Quinolones	1.3929 (122)	1.3812 (240)	1.4483 (176)	1.3513 (203)	1.4353 (109)	1.2391 (135)	0.0117

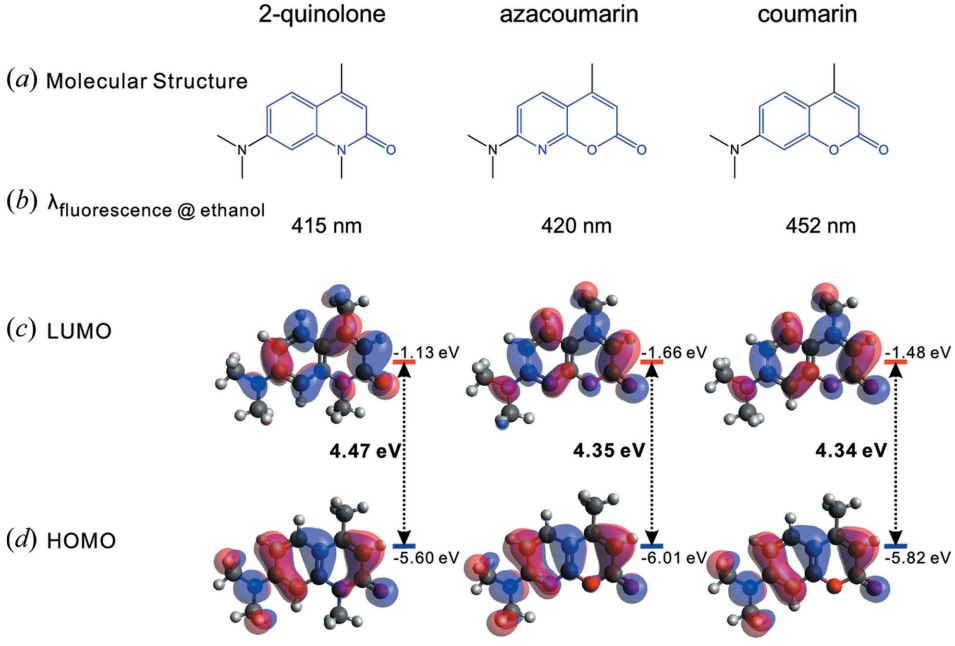

Figure 10
Comparison of selected compounds from the 2-quinolone, azacoumarin and coumarin families. (*a*) Their molecular structures and (*b*) fluorescent wavelengths as measured in *ethanol solution*. (*c*) HOMO and (*d*) LUMO (red: positive; blue: negative; isovalue: 0.02), and the corresponding band gaps of these molecules as computed in the gas phase.

and/or lowering that of the acceptor level in Ring 2 (Duarte & Hillman, 1990). These changes in energy levels can be achieved by attaching different substituents onto both rings and/or replacing certain atoms in the ring framework. As the donor level rises in energy and/or the acceptor level falls, the UV–vis absorption and emission wavelengths for these compounds experience a red shift, as less external energy is required to promote electrons from Ring 1 to Ring 2. Conversely, to tune such wavelengths towards their blue regime, substituents with the opposite electron-donating/-withdrawing strengths should be adopted.

Compared with coumarins, *para*-quinoidal Ring 1 in azacoumarins has lower ground-state energy, as indicated by the higher ionization potential of pyridine relative to that of benzene (Hammond *et al.*, 1975). This is equivalent to decreasing the donor-level energy of Ring 1, thereby leading to larger band gaps in azacoumarins. Consequently, the wavelengths of azacoumarins experience a strong blue shift compared with their coumarin analogues. This effect is probably best illustrated by considering the fluorescent wavelengths of the three classes of chemical families shown in Fig. 10 (Hammond *et al.*, 1975). While this illustration focuses on fluorescent wavelengths, such conclusions can be equally extended to peak absorption and lasing wavelengths, since absorption, fluorescence and lasing all involve electron transitions between the S_0 and S_1 energy states of these molecules.

Ring 2 acts as an acceptor in 2-quinolones. The substitution of O1 with N1 in this ring reduces its electron-withdrawing power and effectively raises the acceptor energy level. As a result the electronic band gaps of 2-quinolones increase with respect to those of coumarins. In terms of structure, since such an increase makes ICT

Table 6
Average bond lengths of coumarins and 2-quinolones with structural data collected between 180 and 229 K.

	Ring 1						
	Bond *a*	Bond *b*	Bond *c*	Bond *d*	Bond *e*	Bond *f*	Sample size
Coumarins	1.3945 (121)	1.3830 (110)	1.3839 (100)	1.3905 (64)	1.4028 (134)	1.3731 (132)	35
2-Quinolones	1.3917 (49)	1.3773 (41)	1.4000 (50)	1.4070 (60)	1.4078 (41)	1.3747 (31)	6

	Ring 2						
	Bond *g*	Bond *h*	Bond *i*	Bond *j*	Bond *k*	Bond *l*	Bonds *G–H*
Coumarins	1.3832 (91)	1.3729 (158)	1.4469 (165)	1.3591 (200)	1.4425 (115)	1.2098 (74)	0.0102
2-Quinolones	1.3910 (89)	1.3725 (148)	1.4610 (195)	1.3550 (93)	1.4428 (105)	1.2395 (161)	0.0185

Table 7
Average bond lengths of coumarins and 2-quinolones with structural data collected between 273 K and 300 K.

	Ring 1						
	Bond *a*	Bond *b*	Bond *c*	Bond *d*	Bond *e*	Bond *f*	Sample size
Coumarins	1.3953 (171)	1.3844 (175)	1.3834 (140)	1.3921 (111)	1.4036 (148)	1.3741 (151)	514
2-Quinolones	1.3865 (130)	1.3761 (174)	1.3988 (159)	1.4028 (122)	1.4034 (113)	1.3702 (137)	106

	Ring 2						
	Bond *g*	Bond *h*	Bond *i*	Bond *j*	Bond *k*	Bond *l*	Bonds *G-H*
Coumarins	1.3788 (106)	1.3773 (137)	1.4424 (162)	1.3500 (179)	1.4386 (146)	1.2083 (109)	0.0014
2-Quinolones	1.3900 (121)	1.3803 (200)	1.4498 (158)	1.3590 (215)	1.4362 (134)	1.2369 (160)	0.0097

from Ring 1 and Ring 2 more difficult, the *para*-quinoidal pattern is not observed in (3).

These qualitative relationships are supported by TD-DFT calculations (Fig. 10). By comparing the HOMOs and LUMOs of compounds from the coumarin, azacoumarin and 2-quinolone families we notice that the charge around the electron-donating substituents at the 7-position is transferred from Ring 1 to Ring 2 upon excitation, as indicated by the diminished electron densities in the LUMOs of these substituents. In addition, the HOMO in azacoumarin (with respect to its LUMO) is lowered relative to that of coumarin, while the LUMO of 2-quinolone (with respect to its HOMO) shows a comparative increase. Consequently, the band gaps of azacoumarin and 2-quinolone are larger than that of the coumarin analogue. Furthermore, there is greater electron density at bond *h* in the ground state of 2-quinolone due to the replacement of O1 with N1. This enhanced electron density reflects the stronger bond character of *h*, agrees with experimental observations on the shortening of this bond and rationalizes the significant resonance structure proposed in Fig. 6 for 2-quinolones. Lastly, it is worth pointing out that the listed fluorescent wavelengths (Fig. 10*b*) do not correspond to the calculated bandgaps (Figs. 10*c* and *d*). The reasons for this disparity are twofold: on the one hand, fluorescent wavelengths are measured in ethanol, while the band gaps are calculated in the gas phase and so this difference somewhat represents solvent effects. On the other hand, the calculations assume a two-state model; in polarisable molecules such as these, however, transitions from multiple orbitals in addition to HOMO-to-LUMO contribute significantly to the overall spectra of these dyes (Cramer, 2002).

4. Concluding remarks

In this study resonance theory has been used to explain the ICT-induced *para*-quinoidal patterns in azacoumarins (1) (LD 425) and (2) (LD 489), and the elongation of bond *l* and shortening of bond *h* in Ring 2 of 2-quinolone (3) (LD 473). In contrast, the *para*-quinoidal resonance state is diminished in (3). The structure of (3) represents the average bond-length pattern shifts of the 2-quinolone family in relation to coumarins.

These structural differences result in comparative blue shifts in the spectra of azacoumarins and 2-quinolones. The replacement of C by N at the 8-position to form azacoumarins effectively reduces the donor-level energy in Ring 1; to form 2-quinolone the ICT effect is suppressed due to the rising acceptor energy level in Ring 2 resulting from changing oxygen to nitrogen at the 1-position. These changes result in large band gaps compared with those of coumarins, as indicated by the variations of their fluorescent wavelengths and corroborated by TD-DFT calculations.

Employing this structural approach to understand laser dye properties is attractive on account of its ability to interpret the wavelength shifts among laser dyes, and do so in an intuitive fashion. This approach also forms a sure foundation for complementary quantum computational calculations which help to gain a more detailed, quantitative understanding of the electron-transfer mechanisms in azacoumarins and 2-quinolones.

APPENDIX *A*
Comparison of average bond lengths in coumarins and 2-quinolones in different temperature groups

Temperature effects have to be taken into account when comparing the bond-length patterns between coumarins and 2-quinolones. At low temperature, apparent bond lengths are longer due to reduced atomic thermal vibrations. In contrast, such vibrations become stronger as temperature increases and this may cause significant bond-length changes. Furthermore, the structural data involved in our statistical analysis were collected at dramatically different temperatures from 90 to 353 K. To minimize the impact of temperature effects, we

divided 653 coumarins and 134 2-quinolones into four different temperature groups – Group 1 between 90 and 129 K, Group 2 between 130 and 179 K, Group 3 between 180 and 229 K, and Group 4 between 273 and 300 K. The bond-length patterns between coumarins and 2-quinolones are compared within each of the groups. (One set of coumarin data collected at 353 K is not included in this grouping as no 2-quinolone data is gathered at such a high temperature for comparison. However, this exclusion should not bias our results, given the large sample size in the remaining groups.)

The structural data of coumarins and 2-quinolones in different temperature groups exhibit the same bond-length patterns. For example, the *para*-quinoidal feature of Ring 1 in coumarins is absent in 2-quinolones, as indicated by the longer average length of bond *c* than that of *b* in 2-quinolones. In addition, bond *l* is relatively longer in 2-quinolones, largely due to the resonance structures between N1 and O2 (Fig. 6). For the same reason, bond *h* is shorter than *g* in 2-quinolones on average. The detailed mean bond distances and associated standard deviations are available in Tables 4–7. The length differences between the average values of bonds *g* and *h* are also presented.

XL is indebted to the Singapore Economic Development Board for a Clean Energy Scholarship. JMC thanks the Royal Society for a University Research Fellowship, the University of New Brunswick (UNB) for The UNB Vice-Chancellor's Research Chair and NSERC for the Discovery Grant, 355708 (for PGW). TCL is indebted to the Taiwanese Ministry of Education for a partially funded PhD studentship. Alisha Cramer from UNB and Jignesh Radia from the Cavendish Laboratory are acknowledged for helpful discussions and assistance. ACEnet, the regional high-performance computing consortium for universities in Atlantic Canada, is also acknowledged for providing computational facilities for this work.

References

Adamo, C. & Barone, V. (1999). *J. Chem. Phys.* **110**, 6158–6170.
Allen, F. H. (2002). *Acta Cryst.* B**58**, 380–388.
Allen, F. H., Kennard, O., Watson, D. G., Brammer, L., Orpen, A. G. & Taylor, R. (1987). *J. Chem. Soc. Perkin Trans. 2*, S1–S19.
Allen, J. R., Biswas, K., Cao, G., Golden, J. E., Mercede, S., Peterkin, T., Reed, A. & Tegley, C. (2009). US Patent App. 20,090/111,806.
Allen, J. R., Burli, R., Bryan, M. C., Cao, G., Neira, S. C. & Reed, A. B. (2009). World Patent WO/2008/130,600.
Atkins, R. L. & Bliss, D. E. (1978). *J. Org. Chem.* **43**, 1975–1980.
Becke, A. D. (1993). *J. Chem. Phys.* **98**, 5648–5652.
Blessing, R. H. (1997). *J. Appl. Cryst.* **30**, 421–426.
Bruno, I. J., Cole, J. C., Edgington, P. R., Kessler, M., Macrae, C. F., McCabe, P., Pearson, J. & Taylor, R. (2002). *Acta Cryst.* B**58**, 389–397.
Butcher, R. J., Jasinski, J. P., Yathirajan, H. S., Narayana, B. & Samshad (2007). *Acta Cryst.* E**63**, o3412–o3413.
Chinnakali, K., Sivakumar, K., Natarajan, S., McGuire, N. K. & Clearfield, A. (1991). *Acta Cryst.* C**47**, 561–563.
Cole, J. M. *et al.* (2011). In preparation.
Cramer, C. J. (2002). *Essentials of Computational Chemistry.* Chichester: John Wiley and Sons.
Dalla Via, L., Marciani Magno, S., Rodighiero, P. & Gia, O. (2002). *Bioorg. Med. Chem. Lett.* **12**, 1253–1257.
Duarte, F. J. & Hillman, L. W. (1990). *Dye Laser Principles, with Applications.* San Diego: Academic Press Inc.
Farrugia, L. J. (1997). *J. Appl. Cryst.* **30**, 565.
Fletcher, A. N., Pietrak, M. E. & Bliss, D. E. (1987). *Appl. Phys. B*, **42**, 79–83.
Frisch, M. J. *et al.* (2009). *GAUSSIAN*09, Revision A.1. Gaussian Inc., Wallingford, CT, USA.
Gilli, G., Bertolasi, V., Bellucci, F. & Ferrett, V. (1986). *J. Am. Chem. Soc.* **108**, 2420–2424.
Hammond, P. R., Fletcher, A. N., Henry, R. A. & Atkins, R. L. (1975). *Appl. Phys.* **8**, 315–318.
Hammond, P. R., Atkins, R. L., Henry, R. A. & Fletcher, A. N. (1978*a*). US Patent 4,103,256.
Hammond, P. R., Atkins, R. L., Henry, R. A. & Fletcher, A. N. (1978*b*). US Patent 4,103,257.
Jasinski, J. P. & Woudenberg, R. C. (1994). *Acta Cryst.* C**50**, 1952–1953.
Kulkarni, M. V., Kulkarni, G. M., Lin, C. H. & Sun, C. M. (2006). *Curr. Med. Chem.* **13**, 2795–2818.
Lapiere, C. (1975). US Patent 3,919,248.
Lee, C., Yang, W. & Parr, R. G. (1988). *Phys. Rev. B*, **37**, 785–789.
Nonius (1998). *COLLECT*. Nonius BV. Delft, The Netherlands.
Otwinowski, Z. & Minor, W. (1997). *Methods Enzymol.* **276**, 307–326.
Rigaku/MSC (2009). *CrystalClear-SM Expert* and *CrystalStructure.* Rigaku/MSC, The Woodlands, Texas, USA.
Schimitschek, E. J. & Trias, J. A. (1976). *Opt. Commun.* **16**, 313–316.
Sheldrick, G. M. (2008). *Acta Cryst.* A**64**, 112–122.
Shimizu, S., Kashino, S. & Haisa, M. (1975). *Acta Cryst.* B**31**, 1287–1292.
Stephens, P. J., Devlin, F. J., Chabalowski, C. F. & Frisch, M. J. (1994). *J. Phys. Chem.* **98**, 11623–11627.
Westrip, S. P. (2010). *J. Appl. Cryst.* **43**, 920–925.
Yang, S.-P., Han, L.-J., Wang, D.-Q. & Xia, H.-T. (2007). *Acta Cryst.* E**63**, o4643.